

PySE: Software for Extracting Sources from Radio Images

D. Carbone^{a,b}, H. Garsden^c, H. Spreeuw^d, J. D. Swinbank^e, A. J. van der Horst^f,
A. Rowlinson^{a,g}, J. W. Broderick^g, E. Rol^{b,i}, C. Law^j, G. Molenaar^a,
R. A. M. J. Wijers^a

^a*Anton Pannekoek Institute for Astronomy, University of Amsterdam, Postbus 94249, 1090 GE Amsterdam, The Netherlands*

^b*Department of Physics and Astronomy, Texas Tech University, Box 1051, Lubbock, TX 79409-1051, USA*

^c*Harvard-Smithsonian Center for Astrophysics 60 Garden Street, Cambridge, MA 02138, USA*

^d*Netherlands eScience Center, Amsterdam, The Netherlands*

^e*Department of Astronomy, University of Washington, Box 351580, Seattle, WA 98195-1580, USA*

^f*Department of Physics, The George Washington University, 725 21st Street NW, Washington, DC 20052, USA*

^g*ASTRON, The Netherlands Institute for Radio Astronomy, Postbus 2, 7990 AA Dwingeloo, The Netherlands*

^h*Monash Centre for Astrophysics (MoCA), Monash University, Melbourne, Victoria, 3800, Australia*

ⁱ*School of Physics and Astronomy, Monash University, Melbourne, Victoria, 3800, Australia*

^j*Department of Astronomy and Radio Astronomy Lab, University of California, Berkeley, CA, USA*

Abstract

PySE is a Python software package for finding and measuring sources in radio telescope images. The software was designed to detect sources in the LOFAR telescope images, but can be used with images from other radio telescopes as well. We introduce the LOFAR Telescope, the context within which PySE was developed, the design of PySE, and describe how it is used. Detailed experiments on the validation and testing of PySE are then presented, along with results of performance testing. We discuss some of the current issues with the algorithms implemented in PySE and their interaction with LOFAR images, concluding with the current status of PySE and its future development.

Keywords: astronomical transients, techniques: image processing, methods: data analysis

1. Introduction

The LOFAR Radio Telescope (van Haarlem et al., 2013) is a radio interferometer comprised of many antennae situated throughout Europe, and linked by a high-speed network. It is one of the new generation radio telescopes, along with the Australian Square Kilometer Array Pathfinder (ASKAP; Johnston et al., 2008), the Murchison Widefield Array (MWA; Tingay et al., 2013), and the Long Wavelength Array (LWA; Ellingson et al., 2009). These telescopes provide high-resolution wide-field imaging,

Email address: dario.carbone@ttu.edu (D. Carbone)

and are proving grounds for the Square Kilometre Array (SKA), which will become the most sensitive radio telescope ever built. LOFAR observes at the low end of the radio spectrum, between 30 and 250 MHz, and its capabilities are being used to support six important projects in radio astronomy, of which transients and variables are one. In order to discover transients, the LOFAR Transients Key Science Project (TKP; Fender et al., 2008) has developed a Transient Pipeline (TRAP; Swinbank et al., 2015) that is able to search for transient and variable sources in an image stream in real time. One of the main steps of this pipeline is the extraction of all the sources present in each image as quickly and as accurately as possible, with a main focus on point sources. Transient sources would very likely be point sources, because a transient typically has a small angular size on the sky, much smaller than the resolution of the instrument. It is within this project that the PySE (Python Source Extractor) has been developed.

Transient signals observed by radio telescopes are generally classified as fast or slow (Cordes et al., 2004; Fender et al., 2008), with the boundary between the two classes set at \sim 1 second, and fast transients occurring down to microseconds. Fast radio transients may be produced by pulsars, gamma ray bursts, flaring stars, and fast radio bursts (Lorimer et al., 2007). Slow transients are produced by large scale high energy events such as flares in quasars, tidal disruption events, and supernovae. There are likely to be unknown transient types in both classes yet to be discovered.

Fast transients are usually too short to appear in an image as their flux would be averaged to very low values; therefore dedicated high speed hardware and software (e.g. Serylak et al., 2013) have been developed to detect them. Slow transients, that appear for long enough to be detectable in a image, can be detected by scanning an image; they will appear as an unknown astronomical object when checked against catalogues (e.g. Stewart et al., 2016; Hyman et al., 2005). This process is therefore one of finding sources in an image, determining their location, brightness, and other parameters, and matching them with known sources. These tasks are well-handled using computer software that detects and characterises sources, and databases that do the data comparison. PySE is an instance of a source finder designed especially for detecting slow transient (i.e. point sources) in a series of images.

This paper describes the functionality of the PySE source finder, presents experimental results indicating how accurate it is, and some performance measures. Section 2 illustrates the reasons for creating a new source finder algorithm, Section 3 describes the program, Section 4 presents different methods to generate simulated maps used to test PySE, Section 5 reports on experiments that demonstrate the accuracy of PySE, Section 6 indicates how PySE performs, and Section 7 discusses our intentions for further use and development.

2. Need for a new source finder

PySE was designed in order to operate as a source finder for the LOFAR Transients Key Project and to be integrated within the TRAP¹.

¹For version 3.0, see <http://tkp.readthedocs.org/en/r3.0/index.html>

Investigations into the acquisition or development of a source finder for the Transients Key Project have been performed and some requirements have been set such as:

- Speed: the source finder should run within few seconds per image. The run-time will depend on the size of the image and on the number of sources, with typical images being around 1024^2 pixels containing about 100 sources corresponding to a run-time of $\lesssim 3$ seconds
- Accuracy: the source finder should calculate the background noise and the source parameters as near as possible to theoretical accuracy limits (background noise within 1 percent, positions within 1 pixel, and fluxes within 5 percent, in absence of noise and within 20 percent in presence of noise and other effects). The source parameters should also have robust error estimates.
- It should be able to handle the correlated noise generated by radio telescopes (Wilson et al., 2012).
- It should be robust, since it will be run as part of an automated imaging and transient-detection pipeline; it must be able to handle images of varying quality, deal with problems, and fail gracefully when failure is absolutely necessary.

Based on these requirements, existing source finders were evaluated as candidates for a LOFAR transients source finder.

2.1. Source finder evaluation, and the impetus for a new source finder

Several programs have been developed for extracting sources from an astronomical image, in most of the cases to fulfill specific requirements of the developers team. Source finders optimised to work on optical or infrared images, e.g. SExtractor (Bertin and Arnouts, 1996) or CuTEx (Curvature Threshold Extractor; Molinari et al., 2011) are not able to deal with correlated background noise that is typical of radio images and were therefore excluded from the candidates for a LOFAR transients source finder because they could not meet our requirements.

Other source finder tools have recently been developed to extract as precisely as possible all the emission present in a radio image, for example PyBDSF (Python Blob Detection and Source Finder, formerly known as PyBDSM; Mohan and Rafferty, 2015), Duchamp (Whiting, 2012), SOURCE_FIND (AMI Consortium et al., 2011), and Aegean (Hancock et al., 2012). These algorithms, which were developed in parallel with PySE, do not focus on the speed of processing large datasets. They proved to be too slow and did not match our speed requirement.

For the above mentioned reasons, it was decided to develop a new algorithm, suited for the purposes of the LOFAR Transients Key Project: PySE.

3. The PySE Program

3.1. PySE design

PySE has been developed to satisfy the requirements described in Section 2. The source-finding algorithms are contained in a stand-alone software package that can also

be integrated into a pipeline, specifically the LOFAR TRAP. PySE is designed to process typical LOFAR images (1024×1024 pixels containing about 100 sources) in 3 seconds (Spreeuw, 2010)². For the processing of images in the TRAP, a real-time, distributed, parallel task scheduling system has been installed, which facilitates the running of many instances of the source finder concurrently, providing the necessary throughput from an automated source-detection pipeline. PySE is built in a high-level programming language, Python, with a modular design, using software engineering practices such as issue-tracking, source control, unit testing, and has been extensively tested (this paper; Rowlinson et al. 2016; Swinbank et al. 2015). It has built-in exception-handling and failure modes.

The source-finding steps are as follows:

1. Find the RMS noise and background over the image and subtract the background map from the original image.
2. Find islands of high pixel values above the noise. From these, create a list of sources for analysis.
3. Deblend islands that may contain multiple sources.
4. Fit parameters to sources. The source parameters are based on 2-D Gaussian fitting to the source.

In order to estimate the background and the noise of an image (Step 1), it is divided into boxes. In each box k , σ clipping around the median is performed until it has converged, i.e., no further pixels are excluded. k , σ clipping has been implemented in PySE slightly differently from SExtractor, by clipping $\pm k\sigma$ around the median instead of $\pm 3\sigma$. The value of k is calculated at each iteration and depends on the number of independent pixels in the image at every step (see e.g., Section 7.1 of the SExtractor manual). At this point the mode and the standard deviation of the distribution of pixels are calculated. The mode is calculated using Equation 1 if the distribution of pixel values is not too skewed otherwise the mode is assumed to be equal to the median, as SExtractor does.

$$mode = 2.5 \times median - 1.5 \times mean. \quad (1)$$

The boundary between these two scenarios is set by the condition in Equation 2.

$$\frac{|mean - median|}{sigma} \leq 0.3. \quad (2)$$

The calculated modes and standard deviations in each box are then interpolated to produce the background and noise maps respectively. The background map is then subtracted from the original image before sources are identified and extracted.

²The software described in (Spreeuw, 2010) discusses a version prior to 3.0, that is identical to what described in this work, apart from the addition of the features of forcing the shape of sources to be the same as the synthesized beam (see Section 3.2) and to extract the flux from predetermined coordinates (see Appendix A).

In order to identify sources (Step 2), the noise map is multiplied by a user specified number (the so-called *detection* threshold). Pixels with a value higher than the local threshold level are considered as source pixels. Once sources have been identified, neighboring pixels with value above another, lower, threshold (determined multiplying the noise map by a user specified number, the so-called *analysis* threshold) are associated to the sources. In case the False Detection Rate algorithm (FDR; Hopkins et al., 2002) is used, the analysis threshold is not calculated and is set equal to the detection threshold. The analysis threshold can never be higher than the detection threshold. The FDR algorithm is a method that allows to impose a maximum fraction of pixels being falsely identified as sources. It calculates internally the best value of the detection threshold to be used in order to fulfill the required limit. The implemented FDR algorithm divides the initial map (after subtracting background) by the noise map. This normalized map is then used to calculate the detection threshold, as explained in Appendix B of Miller et al. (2001). After this, the source extraction works as explained above.

If two or more sources are close enough, they will belong to the same island and will initially be detected as one source. The deblending algorithm (Step 3) implemented in PySE is analogous to the one used by SExtractor. The user specifies the number of subthresholds exponentially spaced between the lowest and the highest pixel value in each island. If the two (or more) sources are separated by any of these subthresholds, they will be recognized as separate sources if in each of them there is at least one pixel with value above the detection threshold.

2-D Gaussians are fitted to the detected sources in order to estimate their positions (right ascension, declination), their shapes (semi-major axis, semi-minor axis and the position angle of the semi-major axis, east from local north) and their brightness (peak flux density), with respective errors. The integrated flux density is reported as well, even if it can be derived from the peak flux density, the size of the axes and the size of the synthesized beam. The fit of the source parameters is performed using a least-squares convergence algorithm, in particular a modified version of the Levenberg-Marquardt algorithm (Moré, 1977). Correlated noise, and errors derived with Gaussian fits in the presence of correlated noise, are implemented from theory (Bertin and Arnouts, 1996; Condon, 1997; Refregier and Brown, 1998; Taylor et al., 1999; Spreeuw, 2010). The user may also request for a residual map, where, for each island, the computed Gaussian has been subtracted from the data.

3.2. PySE Execution

PySE is a standalone Python program that uses the source-finding modules. It is run with several options, followed by a list of input image files, which can be in standard FITS or CASA³ format. On termination the program prints a list of found sources, and may be asked to save information such as the calculated background image, the source list in different formats (e.g. text, region files importable in DS9⁴), and other data requested via command line options.

³www.nrao.com

⁴ds9.si.edu

The main options of PySE are explained in this Section, while a detailed description of all the options is given in Appendix A.

The detection threshold is defined as a multiple of the local noise. Pixels lying above this threshold are defined as sources. Neighbouring pixels brighter than a secondary, lower threshold, the analysis threshold, are grouped into islands and fit to a 2-D Gaussian to extract the source parameters.

The grid size is a very important parameter. It is a value, in number of pixels, that is used in the estimation of the background and the variance map. In order to calculate the noise, the image is split into squared cells of size equal to the grid size. The rms in each cell is calculated and these values are interpolated to create the background mean and variance map. Changing the grid size will therefore potentially affect the noise estimation and the source extraction. The grid size should not be smaller than the size of individual sources, otherwise their flux will dominate the rms calculation in individual cells and be mistaken as noise and both the background mean and variance will be overestimated. It should not be too coarse as well, otherwise the interpolation will not adequately follow the noise pattern in the image. In most cases, i.e. when sources are generally fairly compact or only moderately resolved, a grid size of a few times the most extended source would work adequately.

Another very important option of PySE is the forced clean beam fit. Using this option the shape (major and minor axes and position angle) of the extracted sources is not fit, but forced to be the same as the restoring beam. This implies that all of the extracted sources will have the shape of point sources. This option is especially important in the TRAP. In an image stream a source might appear suddenly much brighter because an image is noisier, and the source finder might misfit it with a much larger 2-D Gaussian introducing artificial variability in the light curve we create in TRAP, making it more difficult to identify real variables. Forcing the shape of the source would fix such issues.

The TRAP will build light curves for all the extracted sources through positional matching. If a source is not detected in an image, either because it is variable or because an image is noisier, the pipeline will extract the flux of that source at its position anyway. This is done using the forced beam shape with fixed position fit option in PySE. This option allows the extraction of the flux at specified coordinates even if there are no pixel values above the detection threshold at that position.

4. Simulations

We used different methods to produce simulated maps to test our software, which are targeted to test particular aspects of the program in detail.

4.1. Method 1: noise and point sources only

First, we want to test the software accuracy in measuring background noise and in recovering sources fluxes and positions. To do so, we have created three types of simulated maps, starting in all cases from the same, real LOFAR observation. All resulting images have 1024×1024 pixels and resolution of about 2.5 arcmin (5 pixels).

The first type is constituted of pure correlated noise, the second contains point sources on a zero background, while the third has point sources on a non-zero background.

In the first case, we empty the image (in the UV plane, therefore preserving the sampling information from the original real observation), generate Gaussian noise with rms 1 Jy in the visibilities and image them by applying a Fourier transform. This way the noise in the image plane is correlated. We produced 10^4 individual maps that will be used to test the accuracy of PySE in estimating the background noise in a radio image.

To produce the second types of maps, we empty the image as in the previous case and insert 100 point sources with flux between 2 and 20 Jy, with the size and shape of the appropriate restoring beam directly in the images. The sources were inserted at random positions, provided they were more than 3 Half Width at Half Maximum (HWHM) apart. These maps therefore have point sources on top of a zero background. They will be used to test the accuracy of PySE in recovering sources fluxes and positions.

In the third case we produced correlated noise, as explained for the first type. After that, 100 point sources, with flux between 2 and 20 Jy and size and shape of the appropriate restoring beam, were added into the images. These maps will be used to test the ability of PySE to retrieve information on sources in a real case, with sources on top of correlated noise.

We have combined the results from the source extraction in each separate image to have statistics on the results in order to avoid having blended sources. We have used these images to validate the code in Section 5.1.

4.2. Method 2: simulating a large number of sources

We have created an entirely different set of simulated images with the only purpose of testing the speed of the algorithm. We created a pixel array containing point sources and random noise, which is then convolved with a clean beam (a 2-D Gaussian) and saved as an image. The images are square, with widths in pixels between 128 and 10240, containing 4 up to 25600 sources. Point sources are placed on a regular grid within the image, so they are equally spaced from each other. The smallest image is of width 128 pixels, containing 4 sources; subsequent images are larger, and have the same density of sources. The grid separation ensures that sources are not blended. While the arrangement of the sources is not astronomical, it is irrelevant for the source finder operations. The fluxes of the point sources are all the same. Since we are only interested in PySE speed, the images have been designed to make the sources all identical (same shape, size and flux) and easy to find (sources are not blended and much brighter than the noise). The full list of images size and number of sources is given in Table 1. These images were used to test the speed of PySE in Section 6.

4.3. Method 3: simulating LOFAR maps

Finally, the last set of simulated images is created to simulate real observations, including, for example, calibration and imaging errors. These simulated images were generated to have several characteristics of real LOFAR data, using the following procedure. We start with an existing LOFAR observation in which we replaced the visibilities with Gaussian noise as in Section 4.1. The standard deviation of the background

Image Width (pixels)	Number of Sources	PySE Run Time (sec)
128	4	1.08
256	16	1.37
512	64	2.57
1024	256	7.68
1536	576	18.74
2048	1024	26.91
3072	2304	58.85
4096	4096	106.59
5120	6400	164.12
6144	9216	239.47
7296	12996	331.67
8192	16384	433.35
9216	20736	525.73
10240	25600	624.89

Table 1: The width of the images used for PySE speed testing, and the number of sources in each image. The number of sources is proportional to the width squared and hence to the total number of pixels.

noise was created to replicate one of a real observation, and as such it depends on the observing frequency, bandwidth, integration time, and configuration of the array when the observation was taken. The noise per baseline (N) is given by:

$$N_{i,j} = \sqrt{\frac{\text{SEFD}_i \times \text{SEFD}_j}{2WI}}, \quad (3)$$

with

$$\text{SEFD} = \frac{2\eta k_B}{A_{\text{eff}}} T_{\text{sys}}, \quad (4)$$

where SEFD_i and SEFD_j are the System Equivalent Flux Densities for each station, W is the total bandwidth, I is the integration time, k_B is the Boltzmann's constant, and η the system efficiency factor (~ 1.0). A_{eff} , the effective collecting area, and T_{sys} , the system noise temperature, are dependent on the array configuration and the observing frequency. In our case, the standard deviation of the background noise is about 1 Jy. We have created our own set of sources to be input in the simulations. This included 100 point sources per image, with fluxes between 2 and 20 Jy. The flux distribution of the sources follow a power-law distribution with exponent equal to -1.5. We added the simulated sources into our dataset using BlackBoard Selfcal (BBS; van der Tol et al., 2007; Loose, 2008). This predicts how the sky model (the list of sources to be inserted) would have been observed by LOFAR given the telescopes gains and frequency used for the original observation.

The simulated data are stored in a Measurement Set (MS); each observation has its own MS, containing all the information pertaining to an observation. An image is

generated by passing the MS through a pipeline consisting of three main steps: flagging, calibration, and deconvolution. Flagging removes bad data from the MS, such as radio-frequency interference and bad data produced by antenna, network, and other failures. Flagging is not necessary for simulated data since bad data are not currently simulated. Calibration adjusts the flux levels of the data so that known sources are matched as closely as possible, thus producing accurate fluxes throughout the rest of the field. In our case, it accounts for noise-induced inaccuracies and allows the simulation to reproduce possible real inaccuracies introduced in this step. Deconvolution (Högbom, 1974) is necessary because the image is blurred by a point-spread-function (PSF) resulting from the small, limited number of antennas that sample the signal; deconvolution removes the side lobes of the PSF and generates the final image. It should be noted that the accuracy of source-finding rests on the accuracy of the aforementioned steps, as source-finding operates on the image produced by them. In our experiments, we assume that these steps have themselves been validated and their accuracy proven. Deconvolution and image generation is performed by AWImager (Tasse et al., 2013). The images created using this method are 512×512 pixels, contain 100 sources each and are used to estimate the best values of the parameters to be used in the TRAP in Section 5.2.

5. The Accuracy of PySE: Validation and Testing

Once images have been made, the next step in transient searches is finding and characterising sources by using a source extraction tool. Two main different steps have been taken to test the source finder performance: the first one is validating the functionality of the source finder itself, while the second consists of the optimization of the parameters used in the source extraction, especially when performed within the TRAP.

All tests performed in this document were performed with the version of PySE incorporated in version 3.0 of TraP, released on 2015-12-14. The software is open source and is publicly available on GitHub as part of the TKP software packages⁵.

5.1. Validation of PySE

We use the simulations described in Section 4 for the validation of PySE. In this section we want to test whether PySE is able to correctly measure the background and the noise in an image. We also test the accuracy of the flux measurements performed by PySE, both in absence and in presence of a background in order to distinguish where the flux uncertainties come from. Finally, we estimate the completeness and reliability of PySE. These parameters have also been calculated in the ASKAP/EMU Source Finding Data Challenge (Hopkins et al., 2015), the results of which are summarized in Section 7. The tests in (Hopkins et al., 2015) cover the performance of PySE on more realistic radio maps, involving crowded fields and presence of extended sources.

We used the simulation procedure described in Section 4.1 for the validation of PySE. In order to validate the software, we want to be sure that the noise measured by

⁵<https://github.com/transientskp/tkp/releases/tag/r3.0rc>

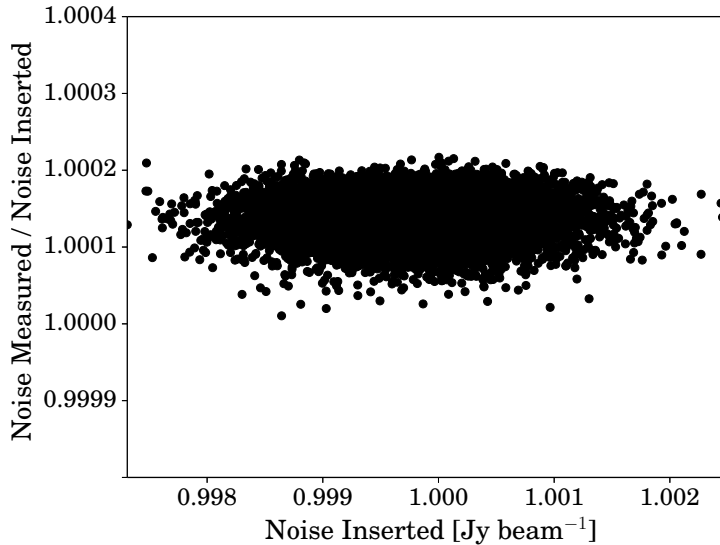


Figure 1: Validation plots of the RMS noise. The vertical axes represents the ratio of the measured and the inserted RMS noise. The scatter around the value of one is less than to 0.1 percent.

PySE is correct. In the TKP pipeline, sources are detected above a threshold defined in terms of the local RMS noise. A robust estimation of the local RMS noise is therefore necessary since any underestimate of the local RMS noise can cause false detections: that is, noise peaks will be incorrectly identified as sources. Therefore we ran tests on 10^4 images produced using maps of the first type described in Section 4.1, in which the RMS of the noise is equal to 1 Jy beam^{-1} . The exact values of the inserted RMS are shown on the horizontal axis of Figure 1 and are calculated as the RMS of the distribution of pixel values in the maps. We then ran PySE on these maps in order to verify that it is able to measure the correct noise from any image. This is done by measuring the RMS of the pixel distribution of the background map generated by the algorithm. The results of this test are summarised in Figure 1 and show that the RMS noise we recover is very similar to the RMS that was injected, with a deviation of less than 0.1 percent. The measured noise is systematically overestimating the inserted one. This can be explained by the fact that image pixels are not normally distributed, despite the fact that the visibilities were. This is probably due to the fact not a proper Fourier Transform is applied, but a gridded Fourier Transform.

The next step is to verify that PySE is able to extract sources at the right locations and with the right parameters (shape and flux). To do this we first produced images with point sources on a zero background. We inserted point sources with fluxes randomly distributed between 2 and 30 Jy. We have tested a total of 40000 sources. The results show that PySE is able to reconstruct the right sources at the right locations and with the right parameters. In Figure 2 we show the recovery of the positions of the extracted sources and their integrated flux. The positions of the sources are measured with very good precision: the position difference is less than 0.1 percent of a beam.

The ratio between the measured and the inserted integrated flux is more spread around 1, even if the discrepancy is well below 5 percent. We note that there are more sources having an underestimated flux rather than overestimated. This is due to the fact that the background mean (i.e. the average of the background noise) is generally overestimated from k , σ clipping due to the presence of sources which cause the background mean to be higher than zero. This background mean is then subtracted leading the measured peak flux densities (and therefore the integrated flux) to be too low. The average source shapes (major and minor axes and position angle of the 2-D Gaussian) and the peak fluxes are reported in the left half of Table 2. We highlight that in this test we do not calculate errors on the extracted parameters because the error calculation (both in fluxes and in positions) is based on the presence of a background noise and therefore not possible. The values of the scatter reported in Table 2 are fluctuations around the mean of all the measurements, not the errors calculated by PySE. These fluctuations (as well as those in the fluxes) are due to differences in the background interpolation: despite we used noise free maps, PySE still performs k , σ clipping, not eliminating all source pixels. These residuals are then interpolated to create a background map that is different for each simulated image. We can see that all of the average values are very close to one. The position angle is less well constrained as the average difference is 9 degrees with a large scatter; this is caused by the fact that the beam in this dataset is almost circular (major/minor axes of the beam = 1.04) and therefore it is harder to constrain its orientation. We have calculated the completeness (fraction of the input sources being detected) and reliability (fraction of the detected sources to be real) for our runs for each simulated image. The completeness is 99.99 percent: 2 sources out of 40000 were not detected. The reliability is always 100 percent.

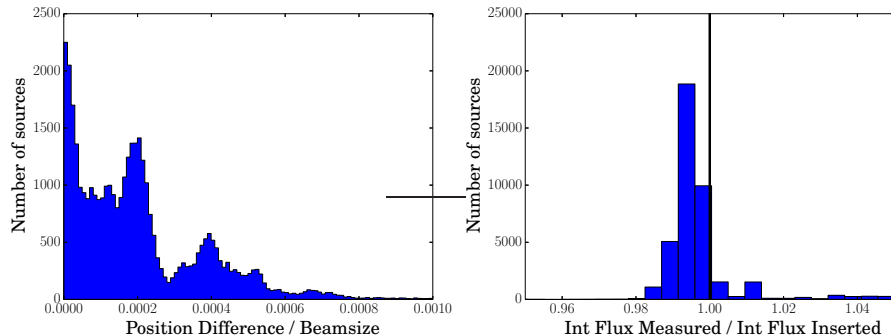


Figure 2: Validation plots of the positions (left panel) and integrated flux (right panel) on a total of 40000 simulated point sources on a zero background. The vertical line in the right panel represents where the ratio between measured and inserted integrated flux is equal to 1.

We then repeat this test with maps in which we added point sources to Gaussian noise. Spreeuw (2010) showed that in the presence of sources, the background noise is overestimated. This is due to the fact that, in the presence of sources, the lower tail of their distribution will mix with the background noise in the image. The contribution of these faint sources will persist in the remaining pixels after k , σ clipping and, since sources are positive defined, they will bias the background mean, resulting in too

much background being subtracted. This effect was already pointed out by Condon (1997), and PySE has implemented a correction to this effect for the peak flux estimation. In our test we added point sources on top of Gaussian noise with RMS equal to 1 Jy beam^{-1} . We inserted point sources with fluxes randomly distributed between 2 and 30 Jy to simulate sources with both a low and a high signal-to-noise ratio. We have set a detection threshold of 5 times the noise so we expect to extract sources brighter than about 5 Jy. The results of our test are shown in Figure 3 for positions and integrated fluxes, and in Table 2 for the average source shapes (semi major, semi minor axes and position angle of the 2-D Gaussian) and peak fluxes, as well as their respective errors. We observe that the scatter around the average value of the parameters reported in Table 2 is higher than the one observed in the noise free case, as expected, but the averages are still close to one apart from the position angle that is not constrained. In particular, we observe that the peak flux ratio is very close to one, despite the aforementioned underestimation of the background, indicating that PySE is able to correct for this effect. We also observe that even if it is still compatible with 1, the semi major axis ratio is on average overestimated. This could be due to the presence of noise which causes the number of pixels associated to each source (pixels with values above the analysis threshold, see Section 3.1) to increase, enlarging artificially the shape of the sources. The same effect is not observed for the semi minor axis. Condon (1997) mentioned the possible presence of biases in recovering Gaussian parameters, particularly at low signal-to-noise. The average difference between the simulated and measured position angle is 66 degrees, with very large scatter. The explanation of this discrepancy is again that the beam shape is almost circular, making more difficult to identify its orientation. Observing the left panel of Figure 3 we can see that the positions are still very well determined. There are a few outliers for which the position difference is around 0.25 beams, which correspond to one pixel. The fluxes are scattered around the inserted values and the spread, measured as the standard deviation of the distribution, is equal to the noise in the maps (1 Jy). The spread is due to the noise is indicated by the two dashed lines in Figure 3. All of the datapoints are consistent with the area delimited by the two lines within 1σ . In the right panel of Figure 3 there seems to be an overestimation in the recovered integrated flux. This is very likely due to the overestimation of the Gaussian parameters, especially the semi major axes, due to the presence of noise as explained above. In fact, we have calculated the average value of the ratio between the measured and the inserted integrated flux, and compared this number to the result of the product of the average ratios of the peak flux, the semi major and semi minor axes, as in Table 2. They are both equal to 1.12, confirming an overestimation of integrated flux, as well as the origin of this effect. We also observe that the integrated flux is overestimated especially at small fluxes, in fact we repeated the calculation of the average ratio between the measured and the inserted integrated flux for sources brighter than 10 Jy and found that this average is equal to 1.05. We have calculated the completeness and reliability also in this case. The completeness depends on the flux of our sources, as we have simulated sources as faint as 2 Jy, but set a detection threshold of 5 times the noise which has an average amplitude of 1 Jy. The overall completeness is 85.2 percent. If we restrict to sources brighter than 5 Jy the completeness is equal to 98.4 percent, for sources brighter than 6 Jy it is 99.8 percent. The overall reliability is 85.8 percent. Considering only bright sources, less likely to be noise peaks, it rises to 98.4

	No Noise		With Noise	
	Average	Scatter	Average	Scatter
Peak flux ratio	0.997	0.009	1.006	0.259
Semi major axis ratio	0.999	0.004	1.112	0.547
Semi minor axis ratio	0.999	0.004	1.001	0.163
Position angle Difference	9 deg	40 deg	66 deg	75 deg

Table 2: Average values and scatter around them of the ratios between the measured and the input values of the peak flux, semi major and semi minor axes, and the difference between the measured and the input values of the position angle of all sources. In the left half we report the result of the test when sources are simulated on top of a zero background (as in Figure 2). In the right half the results refer to the test when sources are simulated on top of correlated noise (as in Figure 3). The scatters are reported at 1σ level.

percent for sources brighter than 5 Jy, and to 99.8 percent for sources brighter than 6 Jy.

As the sources simulated for these tests are all point sources and are created to have the same shape as the restoring beam, we have also tested the use of the forced beam option, which forces all the detected sources to have the same shape (major and minor axis and position angle of a 2-D Gaussian) of the restoring beam. We obtain the same results when we use the forced beam option and when we perform a blind extraction, which confirms that PySE is properly fitting the shape of extracted sources.

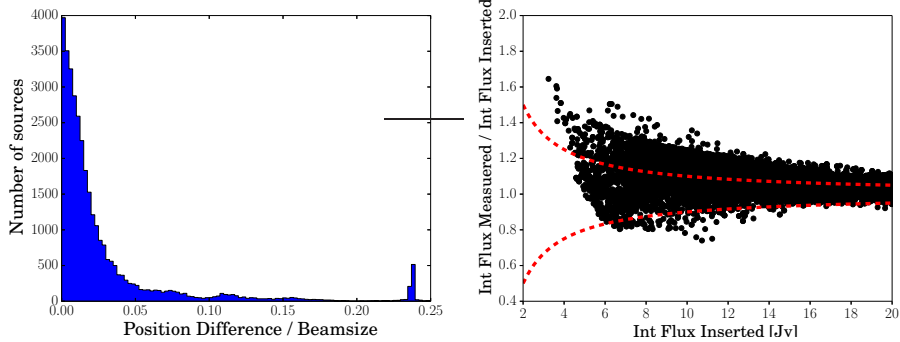


Figure 3: Validation plots of the positions (left panel) and integrated flux (right panel) on a total of 40000 simulated point sources on a non-zero background. The dashed lines in the right panel represent the scatter around a ratio of 1 due to the noise level of 1 Jy beam^{-1} .

In order to test the FDR algorithm in PySE we created 10 different noise maps and for each of them we created 50 different images containing 100, 200, 400 and 600 sources per image to test if the source density would affect the performance of the FDR. The procedure to create the images used for this test is the same we used earlier, i.e., maps of the third type in Section 4.1. The source fluxes varied between 1 and 20 Jy. We tested the performance by varying the maximum percentage of false detections (α), with values of 0.1, 0.05, 0.01, 0.005, 0.001, 0.0005, 0.0001, 0.00005, 0.00001, 0.000005, and 0.000001. We then compared the output source list of PySE with the input catalog and calculated the percentage of falsely detected pixels we obtained. The results of this test are shown in Figure 4. We can see that a fraction of less than 10^{-6}

false positives was not achieved. Moreover, we note the measured value of the False Detection Rate is systematically smaller for smaller source density, and with 400 and 600 sources per image, a fraction of less than 10^{-5} false positives was not achieved. This is due to the fact that a higher ratio between the number of background pixels and source pixels helps obtaining a more accurate noise map with which the FDR algorithm calculates the threshold to be used in the source extraction. This implies that when using the FDR algorithm one has to be aware of the density of sources in the analyzed field in order to use an adequate limit that the algorithm can support.

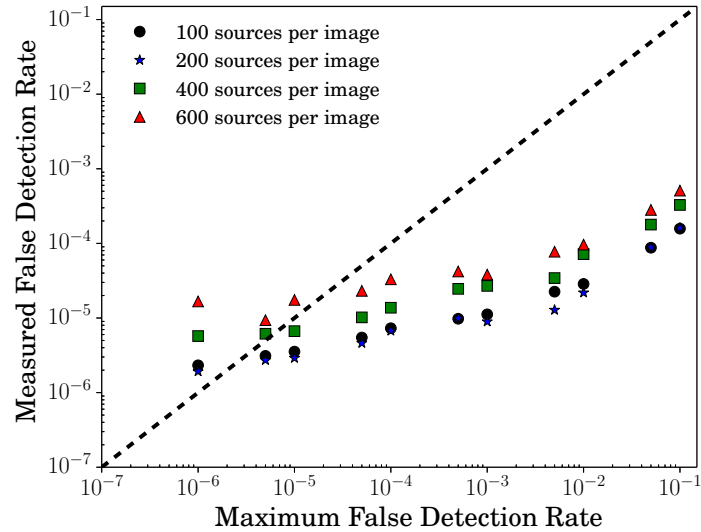


Figure 4: Results of the test of the False Detection Rate algorithm. We note that the recovered value of the False Detection Rate is systematically smaller for smaller source density, implying that the success of the algorithm depends on the density of sources in the image. The dashed line represents the one-to-one relation. We can see that false detection rates as low as 10^{-6} are not achieved.

The final test we did concerned the accuracy of the deblending algorithm, which separates two very close sources in an image. It depends on the distance between sources, on the fluxes of the blended sources with respect to the detection threshold, and on the ratio of the fluxes of two neighbouring sources. To perform this test we created maps inserting Gaussian noise with an amplitude of 1 Jy beam^{-1} and 64 pairs of sources per map with different flux ratios and different separations. The flux of the weakest source was always 20 Jy and the flux ratios were logarithmically spaced between 1 and 1000. This is done to avoid cases where the fainter sources might not be detected due to noise fluctuations; moreover, the ratio between the fluxes of the two components is the most important quantity in disentangling them, together with the angular separation. For every flux ratio 20 maps were processed, each map having a fixed separation between the two sources in each of the 64 pairs. The separations corresponding to each of the 20 maps were linearly spaced between 2 and 7 Gaussian widths. For the source detection we chose a 10σ detection threshold and a 3σ analysis threshold. The conclusion was that up to about 30 percent more sources can be detected

with the deblending algorithm than when it is not used.

For further details on these tests, see chapter 3 of Spreeuw (2010).

5.2. PySE parameters in the Transient Pipeline

One of the most important reasons for developing PySE is its implementation into the LOFAR TRAP⁶. We have performed a study of the PySE source finder software to determine the best values of the parameters that should be used in the TRAP version 3.0. We have done tests on both simulated and real LOFAR maps. The simulations used in this case were created following the method described in Section 4.3.

The images used for this test are not as simple as the ones used so far because they are possibly affected by calibration and imaging errors. This is to emulate the type of real image that TRAP analyses. We have demonstrated in Section 5.1 that the accuracy of PySE in recovering the position of the extracted sources is very good and that the flux recovery is affected especially by the noise RMS. Errors beyond these limits are due to the effects previously listed that affect the accuracy of the recovered parameters. We have used PySE and a tool to do the source matching between the output of PySE and either the sky model from existing catalogues in the case of the real maps, or the input model in the case of the simulated maps. This tool uses a nearest neighbour criterion for the source association, with a cutoff at 3 source HWHM for the association. The final choice of cutoff is rather dependent on the volume and characteristics of the data stream used. We have found that for modest amounts of radio data (of order 10^4 images with each of order 10^6 pixels), an 8σ limit suffices to reduce the number of false positives enough that one can manually investigate their nature, and separate them from real sources. However, far away from the mean the distribution of pixel values is clearly non-gaussian, and the data artefacts vary from instrument to instrument, so we have not yet found automated ways of setting the cutoff - it needs to be done based on close inspection of the data. The simulation images we have analysed have a resolution of about 6 arcmin, with a pixel scale of about 1 arcmin per pixel. This means that a point source would have a full width at half maximum of about 6 pixels. For such configuration, we found that the best value for the grid size parameter in PySE is 50 pixels because it is larger than all the sources in the field, and not coarse either, as explained in Section 3.2. We would like to stress that the best value for the grid size might be very different than the one we quote here, depending on the pixel scale and the beam parameters of the dataset, and the eventual presence of extended emission.

In the TRAP, the association between extracted sources and catalogue sources is performed using the De Ruiter Radius criterion (de Ruiter et al., 1977). The De Ruiter Radius takes into account the coordinates of the source to be associated and their errors:

$$R_{DR} = \left(\frac{\Delta[\alpha \cdot \cos(\delta)]^2}{\sigma_\alpha^2} + \frac{\Delta(\delta)^2}{\sigma_\delta^2} \right)^{1/2}. \quad (5)$$

⁶ Although TRAP was designed and developed within the LOFAR TKP, it has now been used with data from other telescopes, e.g., MWA (Rowlinson et al., 2016) and VLITE (Polisensky et al., 2016).

$\Delta[\alpha \cdot \cos(\delta)]$ and $\Delta(\delta)$ represent the difference between the coordinates of the same source as extracted by the source finder and as tabulated in the catalog, and σ_α and σ_δ represent the errors in the measurements of the coordinates of the source in the extraction by the source finder. As the De Ruiter Radius is inversely proportional to the position errors, this means that sources of which positions are measured with great precision will have large values for the De Ruiter Radius. This affects especially bright sources because their positions can be measured with better accuracy than fainter ones, and can be a problem because it can happen that very bright sources in an image are not associated. Sources can be detected not at their nominal position because of scintillation, an effect that cause the position of sources to move. In the TRAP sources with a De Ruiter Radius lower than 5.68 are associated, otherwise they are not. This choice corresponds to the probability of mis-associating sources of $1:10^6$. In our source association results we looked for sources that should be associated but have a De Ruiter Radius above 5.68. We then added systematic uncertainties of 1/4 pixel, 1/2 pixel and 1 pixel size, and examined its effect on the De Ruiter Radius. We concluded that a systematic error of 1/2 pixel is sufficient to associate the brightest sources correctly. In Section 5.1 we have demonstrated PySE is very accurate in recovering the position of the extracted, therefore the missing associations are due to other effects, such as scintillation due to the ionosphere. More realistic simulations, including ionospheric effects, will be necessary to better determine the systematic errors needed in our pipeline.

As part of our tests we also checked the flux recovery in both our simulated and real maps. All our simulated maps indicated that the flux uncertainty for the sources in there was ~ 20 percent for all fluxes. This amount can vary for a different dataset. In Section 5.1 we proved that the accuracy of PySE in the flux recovery is affected by the amplitude of the standard deviation of the background noise, an effect that is not proportional to the flux of the source, and by the background mean estimation. The uncertainty measured in real maps is therefore caused by a combination of calibration errors, imaging artefacts and ionospheric effects.

Finally, we demonstrated the functioning of the FDR algorithm, and we have proven that its performance depends on the source density. We have therefore decided not to use it as a standard input in the TRAP because we do not know the number density of sources in the images *a priori*, and therefore we cannot be sure if the maximum fraction of false detections will be met.

6. Speed Performance of PySE

Experiments were carried out to evaluate the run-time of a single-processor execution of PySE when images of different sizes, with different numbers of sources, are used and the speedup that can be gained on the same images when multiple concurrent processes are used. For these tests we used only images that were simulated using the technique described in Section 4.2. Sizes, number of sources and run-times of the images we used in this Section are reported in Table 1.

PySE was run on a node of the LOFAR cluster which has 8 CPUs for parallel runs, using the parameters determined to be the best for standard LOFAR images (see Section 5.2). In Table 3 we report the specifications of the machine on which the performance tests were executed.

Architecture	x86_64
CPU op-mode(s)	32-bit, 64-bit
CPU(s)	8
Thread(s) per core	1
Core(s) per socket	4
CPU socket(s)	2
NUMA node(s)	1
Vendor ID	GenuineIntel
CPU family	6
Model	23
Stepping	10
CPU MHz	2003.000
Virtualisation	VT-x
L1d cache	32K
L1i cache	32K
L2 cache	6144K

Table 3: The specification of the machine on which PySE was run for performance tests.

Only the run-time will be reported for all tests. There are two run-times recorded for each image: one is the total program run-time and the other is the run-time of the parallel sections only. The PySE experiments varying the number of sources use the former; the latter is relevant only for the speedup tests.

The sections of the algorithm that are parallelized are:

- Calculation of the background noise in different boxes. The analysis of different boxes can be shared among processes.
- Extraction of islands of pixels to be analyzed. Once a peak over the detection threshold is found, neighboring pixels are associated to the same island. This step includes deblending sources as well. The analysis of different islands can be shared among processes.
- Extraction of source parameters by Gaussian fitting. Once a set of true sources are found, their parameters are determined. The analysis of different islands can be shared among processes.

We note that there is another factor that can affect the speed performance of PySE is the presence of blended sources, i.e. more sources falling in the same island. PySE is able to distinguish them by applying a series of logarithmically spaced sub-thresholds that will separate the two peaks. We did not quantify how it would affect the performance of the algorithm because it is difficult to quantify the amount of blending. A series of factors are playing a role here. For example, how close the peaks are (both in space and in relative brightness) and how many peaks are blended in the same island. The most important parameter to take into account here is the number of deb lancing thresholds to be used. The more sources are blended, the higher the number of sub-threshold should be to distinguish them, the slower the run will be.

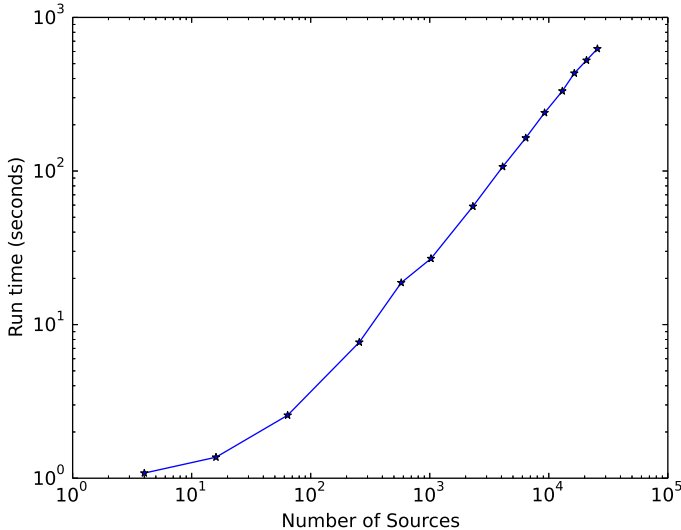


Figure 5: Run-time of PySE as a function of the number of sources in the image. The run-time increases almost linearly with the number of sources, for a number of sources greater than ~ 100 . The slope in the log-log scale between 64 and 25600 sources is equal to 0.92.

6.1. Results

6.1.1. Number of Sources

Figure 5 shows how the run-time of non-parallel (single process) PySE increases as the number of sources increases. The graph shows a close-to linear relationship for a number of sources greater than ~ 100 . This means that the overhead time is negligible in most of the datapoints. In order to calculate the overhead time, we ran an instance of PySE on an image containing a single source and found a runtime equal to 0.95 seconds, most of this being time for startup, image loading, background estimation, and other initial and final tasks that are not parallelised. A linear relationship is the best that can be expected, and PySE approximately reaches this, in fact the slope of the curve in log-log space for a number of sources greater than 64 is equal to 0.92.

We also note that for a number of sources equal to 256 (about twice the amount we expect in a typical LOFAR image) the run time is 7.68 seconds, larger than the requirements we set (3 seconds), but if we extrapolate the value we expect for 100 sources, it is close to the required speed. Further parallelism in the code can help speeding up the code further and fulfill this requirement as well.

6.1.2. Parallel speedup

The top panel of Figure 6 shows the total execution-time speedup that can be gained by increasing the number of processes when PySE is run on a sample of the images used for the previous tests. The parallel speedup is defined as the runtime for 1 processor divided by the runtime for several processes. Ideally, when N processes are used, the speedup should be N , and the program runs N times faster. An ideal speedup is not achieved in Figure 6, mainly due to the fact that only parts of the program can be

parallelised. Larger images with more sources show more speedup, since for smaller images the cost of managing parallel processes outweighs any benefit that may be obtained, as can be seen for the image containing 4 sources, where there is no speedup.

The bottom panel of Figure 6 shows the speedup for just the sections of code that have been parallelised. When there is a small number of sources, the overhead of managing the parallel code sections means that little speedup is achieved. However, with a large number of sources, the overheads are small compared to the amount of work to be done, and sharing the work among several processes reduces the run-time considerably. For example, when there are 4096 sources in the image, and 8 processors over which to share the work, the run-time is reduced by a factor of 6.3.

It is interesting to note that it is not the largest image (25600 sources) that shows the best speedup (that is at 4096 sources); this is because the very largest images meant the operating system started paging, thus degrading performance. In fact, an image size of $\sim 14000^2$ pixels (30000 sources), is the largest image that can be processed, depending on system load.

7. Comparing PySE to other source finding software

Hopkins et al. (2015) conducted the ASKAP/EMU Source Finder Data Challenge comparing the accuracy of many source finders when run on three simulated radio maps containing a mixture of blended, unblended, point and extended sources. Some of the source finding tools that have been tested within the Data Challenge were created to work on radio images, whereas others were designed to work on images at other wavelengths. Despite this, all were tested on the same simulated radio images. The test consisted of three different maps, testing various aspects of the algorithms. The first map (Challenge 1) contained a large number of bright sources with constant number density. The second map (Challenge 2) showed fewer sources but with varying number density across the image in order to mimic the clustering observed in reality. There were more faint sources in this map, to mimic real source counts. Both these maps contained only point sources. The third map (Challenge 3) had the same sources as the second but 20 percent of them were turned into extended ones. These maps were simulations of ASKAP observations. As already mentioned, PySE was designed to detect point sources, and for this reason we decided to focus on retrieving those also in Challenge 3, despite knowing extended emission regions were present. PySE was run using detection and analysis thresholds of 5σ and 3σ respectively. Square cells of side 50 pixels were used for calculating the background and noise maps in Challenges 1 and 2; 30 pixel squares were used for Challenge 3. In each case, we used the option to constrain the shape of the extracted sources to be equal to the restoring beam and to decompose sources lying within the same island.

The results of these tests are summarised in Figures 5, 6 and 7 of Hopkins et al. (2015). PySE achieves a completeness close to 100 percent for sources brighter than 60 mJy in Challenge 1 and a reliability of 100 percent for sources brighter than 40 mJy. In this map the background noise was about 10 mJy/beam. In Challenge 2, where fewer sources were present, the completeness reaches 100 percent at 7 mJy and the reliability at 4 mJy. In this map the background noise was about 1 mJy/beam. In Challenge

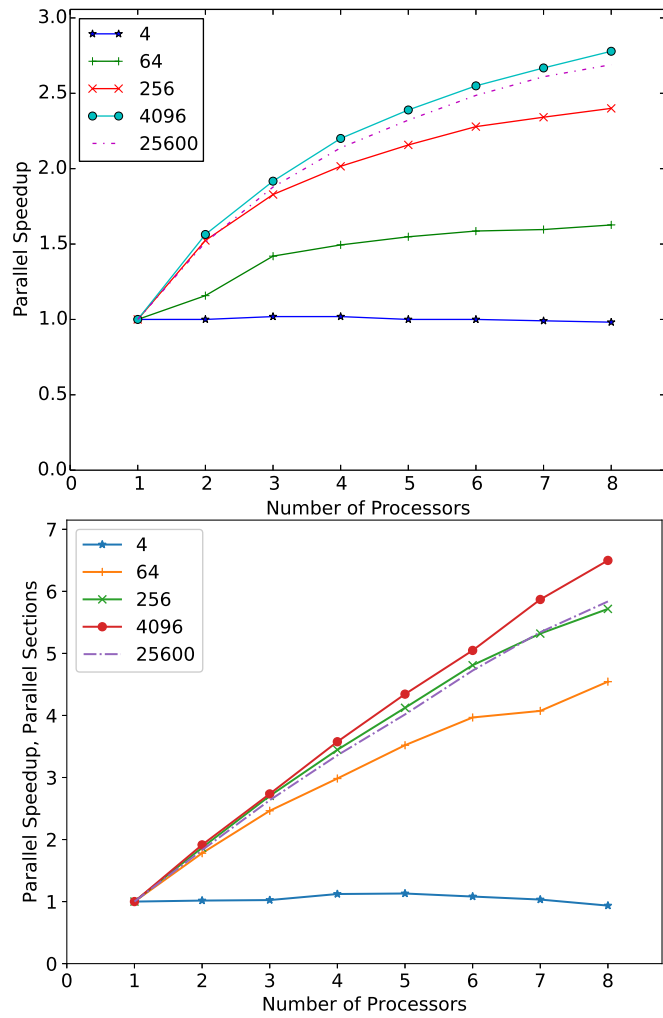


Figure 6: The top panel shows the total speed-up of PySE that can be gained when PySE is run using multiple concurrent processes as a function of the number of sources. The bottom panel regards shows the same relationship, but reporting the speed up of the parallel sections only.

3 PySE did not try to fit the extended emission; despite this, it reaches a completeness of more than 80 percent, meaning that PySE could recognise the brightest part of some of the extended sources as well. The reliability of PySE in Challenge 3 is about 100 percent for sources brighter than 4 mJy. Also in this case, the background noise was about 1 mJy/beam. PySE has been shown to be performing well both in terms of completeness and reliability of the extracted sources, with respect to other source finder algorithms, achieving completeness and reliability close to 100 percent when the signal-to-noise ratio is higher than about 4 in all three challenges.

8. Conclusions

PySE was developed as the source finding algorithm for the LOFAR Transients Key Project in order to extract point sources as quickly and as accurately as possible. Hopkins et al. (2015) has shown PySE to find sources with a high hit rate and low false positive rate. We have shown it to recover sources with accurate locations, fluxes and shape.

PySE has been successfully incorporated as the standard source finding tool of the LOFAR Transients Pipeline. It is able to perform the source extraction in real time, and it is able to cope with the throughput of images generated by LOFAR, thanks to ability of the TRAP to run multiple instances in parallel.

PySE was designed to efficiently detect and deal with point sources within the TRAP, for example, it can force the shape of the extracted sources to be the same as the one of the restoring beam. Another important option of PySE is the forced extraction. This allows the user to specify a list of coordinates where PySE must extract the flux of a point source even if a source at that location has not been found. This is very important in order to monitor the flux of a newly detected source.

We have analysed the usage of the False Detection Rate algorithm and showed that its performance is varying according to the source density of the field. For this reason we have decided not to use it within the TRAP, although we maintain this functionality for when PySE is operated as a standalone tool.

In real maps the errors in the positions and the fluxes recovered by PySE are much larger than the ones we measured on simulated maps. The origin of these larger errors is attributed to factors other than PySE, such as ionospheric effects, calibration errors and imaging artefacts.

We have demonstrated that the speed of PySE is scaling near-linearly for large numbers of sources when the overhead time becomes negligible. Moreover, there are parts of the code that can be parallelised, increasing the performance of the code further.

A comparison of the accuracy of PySE with other source finders has been performed by the ASKAP Source Finder Challenge (Hopkins et al., 2015). PySE has been shown to perform well compared to other algorithms in completeness, reliability and accuracy of the recovered source parameters.

Acknowledgments

LOFAR, the Low Frequency Array designed and constructed by ASTRON, has facilities in several countries, that are owned by various parties (each with their own fund-

ing sources), and that are collectively operated by the International LOFAR Telescope (ILT) foundation under a joint scientific policy. DC, RAMJW, AR, GM. acknowledge support from the European Research Council Advanced Grant 247295 “AARTFAAC”. HG conducted this work at CEA Saclay, France, and acknowledges financial support from the UnivEarthS Labex program of Sorbonne Paris Cit  (ANR-10-LABX-0023 and ANR-11-IDEX-0005-02). This work utilises a number of PYTHON libraries, including the MATPLOTLIB plotting libraries (Hunter, 2007), NUMPY (van der Walt et al., 2011) and SciPy (Jones et al., 2001).

Appendix A. List of PySE options

The options that can be used when running PySE are:

- fdr: use of the False Detection Rate (FDR) algorithm to determine the detection threshold to be used in the source extraction process.
- alpha: maximum allowed percentage of false detections in the FDR.
- detection: detection threshold, given as a multiple of the noise. The detection threshold is a factor that, multiplied by the noise map, sets the minimum flux density that a pixel must have to be recognised as a source.
- analysis: analysis threshold, given as a multiple of the noise. Once a peak is detected, neighbouring pixels will be analysed and if they lie above the analysis threshold they are grouped as part of the same source.
- grid: size of the squares in which the image is divided, in pixels. The image is divided into pieces in which the background and noise are calculated and then interpolated to create the background map on top of which sources are detected. This parameter is very important because the grid has to be not too fine, otherwise a single source can dominate the background in certain parts, nor too coarse otherwise variations in background and noise across the image will not be properly traced.
- margin: margin on each side of the image that will not be analysed, in pixels.
- radius: radius from the centre of the image that will be analysed, in pixels.
- detection-image: finds sources on a different image than the one where fluxes are extracted. To compensate for the increasing noise towards the edges, it is possible to use a non-primary beam corrected image as image in which sources are detected and then a primary beam corrected one for the calculation of their fluxes.
- deblend: use the deblending algorithm. This option requests that the program disentangle two or more sources lying in the same island. An island is a group of pixels with fluxes above the analysis threshold, with at least one pixel above the detection threshold.
- deblend-thresholds: number of logarithmically spaced deblending subthresholds.
- force-beam: force fit axis lengths to beam size. This option does not allow the software to fit the shape of the sources but instead, when a source is found, its shape is immediately fixed to the shape of the beam. This means that using this option every source that is extracted is assumed to be a point source.
- bmaj: major axis of the beam, in degrees.
- bmin: minor axis of the beam, in degrees.
- bpa: position angle of the beam, in degrees.

--fixed: specify coordinates where a source is assumed to be, even if a source at that location has not been detected. This is very important in case a transient source appears because we want to build its light curve from the beginning of our observations and after its disappearance. Coordinates are given as a list in J2000 format, in decimal degrees.
--fixed-list: specify a file containing a list of positions to force the source extraction.
--ffbox-in-beampix: specify positional freedom/error-box size for forced source extraction. Given as a multiple of beam width.
--regions: generate DS9 region file(s).
--csv: generate csv text file containing information about the extracted sources.
--sky model: generate sky model file that could be used in BBS or in Default Pre-Processing Pipeline for self calibration, containing information about the extracted sources.
--residuals: generate residual maps to check whether the source extraction was successful.
--islands: generate island maps to check where the extracted sources are.
--rmsmap: generate RMS map of the background to check the noise level in the image.
--sigmap: generate significance map to check the signal-to-noise ratio of each pixel compared to the local RMS noise.

A review of the program and its options is given in the PySE Manual⁷.

References

References

- AMI Consortium, Franzen, T. M. O., Davies, M. L., et al., Aug. 2011. 10C survey of radio sources at 15.7 GHz - I. Observing, mapping and source extraction. *MNRAS* 415, 2699–2707.
- Bertin, E., Arnouts, S., Jun. 1996. SExtractor: Software for source extraction. *A&AS* 117, 393–404.
- Condon, J. J., 1997. Errors in elliptical Gaussian fits. *PASP* 109, 166–172.
- Cordes, J. M., Lazio, T. J. W., McLaughlin, M. A., Dec. 2004. The dynamic radio sky. *NAR* 48, 1459–1472.
- de Ruiter, H. R., Willis, A. G., Arp, H. C., 1977. A Westerbork 1415 MHz survey of background radio sources. II - Optical identifications with deep IIIA-J plates. *A&AS* 28, 211–293.
- Ellingson, S. W., Clarke, T. E., Cohen, A., et al., Aug. 2009. The Long Wavelength Array. *IEEE Proc.* 97, 1421–1430.

⁷<http://tkp.readthedocs.org/en/r3.0/tools/pyse.html>

- Fender, R., Wijers, R., Stappers, B., LOFAR Transients Key Science Project, May 2008. LOFAR Transients and the Radio Sky Monitor. arXiv:0805.4349.
- Hancock, P. J., Murphy, T., Gaensler, B. M., et al., May 2012. Compact continuum source finding for next generation radio surveys. *MNRAS* 422, 1812–1824.
- Högbom, J. A., 1974. Aperture Synthesis with a non-regular distribution of interferometer baselines. *A&AS* 15, 417–426.
- Hopkins, A. M., Miller, C. J., Connolly, A. J., et al., Feb. 2002. A New Source Detection Algorithm Using the False-Discovery Rate 123, 1086–1094.
- Hopkins, A. M., Whiting, M. T., Seymour, N., et al., Oct. 2015. The ASKAP/EMU Source Finding Data Challenge. *PASA* 32, e037.
- Hunter, J. D., 2007. Matplotlib: A 2d graphics environment. *Computing In Science & Engineering* 9 (3), 90–95.
- Hyman, S. D., Lazio, T. J. W., Kassim, N. E., et al., Mar. 2005. A powerful bursting radio source towards the Galactic Centre. *Nature* 434, 50–52.
- Johnston, S., Taylor, R., Bailes, M., et al., Dec. 2008. Science with ASKAP. The Australian square-kilometre-array pathfinder. *Experimental Astronomy* 22, 151–273.
- Jones, E., Oliphant, T., Peterson, P., et al., 2001. SciPy: Open source scientific tools for Python.
- Loose, G. M., Aug. 2008. LOFAR Self-Calibration Using a Blackboard Software Architecture. In: Argyle, R. W., Bunclark, P. S., Lewis, J. R. (Eds.), *Astronomical Data Analysis Software and Systems XVII*. Vol. 394 of *Astronomical Society of the Pacific Conference Series*. p. 91.
- Lorimer, D. R., Bailes, M., McLaughlin, M. A., et al., Nov. 2007. A Bright Millisecond Radio Burst of Extragalactic Origin. *Science* 318, 777–.
- Miller, C. J., Genovese, C., Nichol, R. C., Wasserman, L., Connolly, A., Reichart, D., Hopkins, A., Schneider, J., Moore, A., Dec. 2001. Controlling the False-Discovery Rate in Astrophysical Data Analysis 122, 3492–3505.
- Mohan, N., Rafferty, D., Feb. 2015. PyBDSM: Python Blob Detection and Source Measurement. *Astrophysics Source Code Library*.
- Molinari, S., Schisano, E., Faustini, F., et al., Jun. 2011. Source extraction and photometry for the far-infrared and sub-millimeter continuum in the presence of complex backgrounds. *A&A* 530, A133.
- Moré, J. J., Jun. 1977. The Levenberg-Marquardt algorithm: Implementation and theory. *Numerical Analysis*. Vol. 630 of *Lecture Notes in Mathematics* 630, 105–116.
- Polisensky, E., Lane, W. M., Hyman, S. D., Kassim, N. E., Giacintucci, S., Clarke, T. E., Cotton, W. D., Cleland, E., Frail, D. A., Nov. 2016. Exploring the Transient Radio Sky with VLITE: Early Results 832, 60.

- Refregier, A., Brown, S. T., Mar. 1998. Effect of Correlated Noise on Source Shape Parameters and Weak Lensing Measurements. arXiv:9803279.
- Rowlinson, A., Bell, M. E., Murphy, T., et al., Jun. 2016. Limits on Fast Radio Bursts and other transient sources at 182 MHz using the Murchison Widefield Array. *MNRAS* 458, 3506–3522.
- Serylak, M., Karastergiou, A., Williams, C., et al., Mar. 2013. Observations of transients and pulsars with LOFAR international stations and the ARTEMIS backend. In: IAU Symposium. Vol. 291 of IAU Symposium. pp. 492–494.
- Spreeuw, J. N., 2010. Search and detection of low frequency radio transients. Ph.D. thesis, University of Amsterdam.
- Stewart, A. J., Fender, R. P., Broderick, J. W., et al., Mar. 2016. LOFAR MSSS: detection of a low-frequency radio transient in 400 h of monitoring of the North Celestial Pole. *MNRAS* 456, 2321–2342.
- Swinbank, J. D., Staley, T. D., Molenaar, G. J., et al., Jun. 2015. The LOFAR Transients Pipeline. *A&C* 11, 25–48.
- Tasse, C., van der Tol, S., van Zwieten, J., van Diepen, G., Bhatnagar, S., 2013. Applying full polarization A-Projection to very wide field of view instruments: An imager for LOFAR. *A&A* 553, A105.
- Taylor, G. B., Carilli, C. L., Perley, R. A. (Eds.), 1999. Synthesis Imaging in Radio Astronomy II. Vol. 180 of Astronomical Society of the Pacific Conference Series.
- Tingay, S. J., Goeke, R., Bowman, J. D., et al., Jan. 2013. The Murchison Widefield Array: The Square Kilometre Array Precursor at Low Radio Frequencies. *PASA* 30, 7.
- van der Tol, S., Jeffs, B. D., van der Veen, A.-J., Sep. 2007. Self-Calibration for the LOFAR Radio Astronomical Array. *IEEE Transactions on Signal Processing* 55, 4497–4510.
- van der Walt, S., Colbert, S. C., Varoquaux, G., 2011. The numpy array: A structure for efficient numerical computation. *Computing in Science & Engineering* 13 (2), 22–30.
- van Haarlem, M. P., Wise, M. W., Gunst, A. W., et al., Aug. 2013. LOFAR: The Low-Frequency ARray. *A&A* 556, A2.
- Whiting, M. T., Apr. 2012. DUCHAMP: a 3D source finder for spectral-line data. *MNRAS* 421, 3242–3256.
- Wilson, T. L., Rohlfs, K., Hüttemeister, S., Dec. 2012. Tools of Radio Astronomy, 5th edition.